



ELSEVIER

Contents lists available at ScienceDirect

Computational Materials Science

journal homepage: www.elsevier.com/locate/commatsci



Dendritic growth of high carbon iron-based alloy under constrained melt flow



Weiling Wang, Sen Luo, Miaoyong Zhu*

School of Materials and Metallurgy, Northeastern University, Shenyang 110819, China

ARTICLE INFO

Article history:

Received 7 April 2014

Received in revised form 5 July 2014

Accepted 10 July 2014

Available online 9 August 2014

Keywords:

High carbon iron-based alloy

Dendritic growth

Melt flow

Cellular automaton

Block-corrected TDMA method

ABSTRACT

A cellular automaton (CA) model coupled with momentum, mass and heat transport models was developed to investigate equiaxed and columnar dendritic growth of Fe–0.82 wt% C alloy under four elaborately designed forced flows. During the iterative solution, the evolution of solidification interface and the solute diffusion in solid phase were explicitly tracked and solved, while other transport equations were implicitly solved in staggered grids with the block-corrected TDMA approach. The self-developed codes show a good performance in predicting dendritic growth and melt flow and temperature fields according to the comparisons with LGK analytical model and commercial software. The growth behavior of dendrites under melt flow is determined by the competition between bringing in solute enriched melt from upstream side and carrying away solute rejected at interfaces. The growth of equiaxed dendrites is promoted at the upstream side and inhibited at the downstream side, which becomes more significant with the increase of inlet velocity and the decrease of melt undercooling. Meanwhile, the oblique flow plays an important role in the growth of arms at the downstream side and alleviates the inhibited growth at the lower melt undercooling. Columnar dendrites are under inhibited growth in sequence along the flow direction, except that those near the outlet are promoted under weaker melt flow. Secondary dendrite arms firstly well formed at left sides of columnar dendrites become fatter and better developed compared with those without flow, although those near the upstream side are difficult to be developed. Under the circular flow condition, columnar dendrites at the bottom wall of the modeling domain firstly grow faster than those symmetrically in the right wall, and then become slower as the solidification proceeds under stronger melt flow. Moreover, the effect of melt flow on dendritic growth becomes more significant under the lower melt undercooling condition for equiaxed dendrites and the weaker cooling condition for columnar dendrites. In addition, compared with the effect on the temperature distribution, the effect of the melt flow on the solute distribution around columnar dendrites governs their growth.

© 2014 Elsevier B.V. All rights reserved.

1. Introduction

During the solidification of alloys, the melt flow as an inevitable phenomenon is customarily induced by the intrinsic characteristics of alloy solidification such as thermal and solutal variations in die casting process and the external forces such as pouring and electromagnetic stirring (EMS) in continuous casting process [1]. The melt flow not only influences dendritic growth, morphology and distribution of grains and solute distribution in the microscopic and the mesoscopic scale, but also determines solute migration and segregation in the macroscopic scale, and thus plays a critical role in the inner solidification quality of alloy ingots and strands. Moreover, the effect of melt flow on dendritic growth is

characterized by dendritic growth direction, primary and secondary dendrite arm spacings and liquid fraction of the porous mushy zone and ultimately exerts on the compactness of columnar and equiaxed dendrite zones, known as the permeability of the mushy zone [1,2], which is the key parameter to accurately investigate the formation and the development of macro segregation. Therefore, the investigation of the dendritic growth of alloys under melt flow during the solidification process is an important and necessary step for the further insight into the formation mechanism of solidification defects and contributes much to control and improve the solidification quality of alloys.

Beckermann and his coworker [3–5] proposed that numerical modeling of dendrite solidification under melt flow should incorporate the microscopic phenomena such as nucleation and dendritic growth and the macroscopic transport phenomena. They were the first to couple classical analytical theories of dendritic

* Corresponding author. Tel.: +86 24 8368 6995.

E-mail address: myzhu@mail.neu.edu.cn (M.Y. Zhu).

growth with momentum, heat and mass conservation equations based on the volume averaging approach [6] and they developed a delicate and reasonable mathematical model for equiaxed dendrite solidification which was validated according to experimental results of Al–4 wt%Cu alloy and NH₄Cl–H₂O solution. This method was appropriate to simulate the solute distribution in the macroscopic scale and the formation of macro segregation. However, since the equiaxed dendrite was assumed to be spherical in the model, the effect of melt flow on the morphology and the growth behavior of dendrites could not be described precisely. Fortunately, as phase field method [7–13], front tracking method [14–17] and stochastic methods such as CA approach [18–39] were introduced, the evolution of solidification interface could be tracked directly or indirectly according to physical variables, so that the microscopic solidification phenomena and related parameters could be qualitatively represented and quantitatively predicted, respectively, as well as the influence of transport phenomena such as the melt flow. These researches were mainly carried out through coupling momentum and mass conservation equations of the melt fluid with the growth kinetic equations of dendrites in the microscopic scale.

Phase field approach was the first to be employed to investigate the impact of melt flow on the growth behavior of equiaxed dendrites of pure materials in two dimensional (2D) domains, and then was extended to the application in three dimensional (3D) domains and binary alloy systems [7–9]. Lan and Shih [10] developed a 2D phase field model with adaptive meshes to investigate the growth behavior of equiaxed dendrites of Ni–Cu alloy in under-cooled melt under forced flow and non-isothermal conditions and found that the upstream dendritic arm grew faster with more developed secondary dendrite arms compared with other ones. Chen et al. [11] developed 2D and 3D phase field models and analyzed different influences of melt flow on the growth behavior of equiaxed dendrites controlled by the thermal diffusion. Zimmermann et al. [12] used the flow field calculation software CrysMAS and the phase-field code MICRESS to investigate the effect of melt flow on the growth behavior of columnar dendrites of AlSi₇ based alloys during the directional solidification process and presented the asymmetric dendritic morphology under melt flow. Guo et al. [13] adopted the parallel-multigrid approach to solve the coupled thermal-solutal-convective equations and investigated the phenomena such as dendrite tilting and arm splitting of equiaxed dendrites under melt flow. Since the solute diffusion layers over dendritic branches were sharp during the solidification of alloys, fine meshes in solute diffusion layers were needed to accurately describe the dendrite solidification with phase field approach [14]. In addition, the iterative solution of the momentum conservation equation and the continuity equation would impose more burdens on the computation with finer meshes. Although the adaptive mesh method and the parallel-multigrid approach were introduced, phase field model was still confined to the application in small modeling domains. Therefore, front tracking method [15–17] was employed to simulate the growth behavior of equiaxed dendrites and columnar-to-equiaxed transition (CET) under melt flow. Although it avoided the fine mesh in thermal and solutal diffusion layers, complexity and difficulty induced by explicitly tracking the position of solidification interface hindered its wide application to conditions such as multi-dendritic growth with well developed side branches, let alone under 3D conditions [14].

As a result, CA approach based on the stochastic capture mechanism of interface cell and known for relatively less computational cost, was competent to deal with the coupled problems of transport phenomena with dendritic growth kinetics and of great interest to researchers. Firstly, Shin and Hong [18] developed a CA model to consider the dendritic growth kinetics and introduced the diffusion interface from the phase field model to solve

momentum and mass conservation equations of melt flow, accordingly investigated the growth behavior of equiaxed dendrites of Al–Cu alloy with melt flow. Subsequently, Zhu and her coworkers [19–28] contributed a lot to the development of CA models for dendritic growth and solidification microstructure, especially under melt flow. Zhu et al. [19–22] coupled transport equations directly with the CA model and solved these equations with SIMPLE algorithm and tri-diagonal matrix algorithm (TDMA), accordingly investigated the growth behavior of equiaxed dendrites with different crystal orientations and columnar dendrites of Al–Cu alloys under melt flow. In order to improve solution stability and efficiency of transport equations, Sun et al. [23–27] adopted the Lattice Boltzmann method to solve transport equations and developed CA-LBM and ZS-LBM models with the corporation of different dendritic growth models to describe equiaxed dendritic morphology and solute distribution of binary alloys under natural and forced convection conditions. Coupled with CALPHAD (Calculation of Phase Diagram), the CA-LBM model was extended to equiaxed dendritic growth of ternary alloys with melt convection afterwards [28]. In addition, Liu et al. [29] developed a CA-FDM (Finite Difference Method) model to investigate the effect of stirring melt flow on the morphology of equiaxed dendrites of the Al–Si alloy. Yin et al. [30] also developed a CA-LBM model to investigate the growth behavior of equiaxed dendrites with multi-orientations and the splitting phenomenon of dendritic tips. Recently, Jelinek et al. [31] adopted the parallel computation algorithm and developed a large scale CA-LBM model which showed a good performance in the simulation of the growth behavior of more than ten millions equiaxed dendrites under forced convection. However, the growth kinetics of dendritic growth in above mentioned models was completely based on the linear relationship with the local undercooling or the local liquid concentration at solidification interface, so that, these models neglected the solute balance at solidification interface [32–34]. Shi et al. [35] introduced solute balance equations in separate forms with coordinates [32,33] to determine interface evolution velocity and investigated 3D equiaxed dendritic growth under forced convection and 2D columnar dendritic growth under natural convection in the NH₄Cl–H₂O solution. Meanwhile, Zhang and Zhao [36] employed the normal velocity from solute balance at solidification interface [34] and analyzed the effect of forced convection on equiaxed dendritic growth of Al–Cu alloy under the 3D condition. Li et al. [37] applied a volume averaged technique to predict the evolution of solidification interface according to the solute conservation there and presented the morphology and the solute distribution of equiaxed dendrites of Fe–C alloy under forced melt flow. Lee and his coworkers [38,39] calculated the increase of solid fraction of interface cells directly from equivalent diffusion equations there rather than indirectly from interface velocities, and they developed a CA-FVM (Finite Volume Method) model to investigate the dendrite solidification of binary alloys under natural and forced convection and found that the natural convection induced by the buoyancy would promote the development of secondary dendrite arms of columnar dendrites at the upstream side. Moreover, Karagadde et al. [40] used the volume of fluid (VOF) method and the immersed boundary method (IBM) to track growth and movement of solid dendrites and solve N–S equations and the enthalpy method to deal with the heat transfer problems and investigated the motion and growth behavior of equiaxed dendrites of pure Al under melt flow.

All of the models utilized to describe the effect of melt flow on dendritic growth are on the basis of momentum, heat and mass transport equations and the evolution kinetics of solidification interface. On the one hand, the melt flow field influences solute and temperature distribution in the modeling domain, especially near the solidification interface, and thus changes the growth behavior of dendrites. On the other hand, as dendrite grows, the flow field is

inevitably altered. Therefore, the coupled solution of those equations is of crucial importance to accurately and quantitatively depict dendritic growth behavior with melt flow. Moreover, algorithms for flow field calculation and discrete equations should hold a reliable accuracy to predict the flow field in the domain precisely. Additionally, the thermal diffusion coefficient is about 10^3 – 10^4 times higher than the solute diffusion coefficient, therefore the heat transfer calculation will inevitably reduce the coupled solution efficiency if the explicit method is used [40], giving rise to much difficulty in the simulation of columnar dendrites with forced convection. Two set meshes [14] and implicit solution methods are promising to solve the heat transfer problems. The implicit iteration method common in the SIMPLE algorithm for flow field calculation can describe flow and temperature distribution near solidification interface directly compared with the indirect linear interpolation used in the approach of two set meshes. Remarkably, based on that the iterative solution process is in essence to make solution results meet the conservation of equations, the block-correction technique [41] can promote the convergence of the implicit iteration of implicit equations. Furthermore, phenomena about the growth of equiaxed dendrites under melt flow have been mainly focused on in the past, however numerical researches on columnar dendritic growth under forced convection have seldom been reported.

In present work, a 2D CA-FVM model coupling momentum, mass and thermal transport models with the CA model is developed according to SIMPLE algorithm with staggered grids and FVM method. In the CA model, the Neumann ruler is used, accordingly the neighboring configuration and capture are based on the first four nearest neighbors. The evolution of solidification interface and the solute diffusion of solid phase are explicitly tracked. However, other transport equations are implicitly discretized and solved with block-corrected TDMA method [41]. The capacities of those models are evaluated through comparing with the LGK analytical model [42], adaptive FVM in FLUENT 12.0 and finite element method (FEM) in ANSYS 12.0 (Ansys Inc., Canonsburg, PA). Accordingly, the CA-FVM model is utilized to investigate the growth behavior of equiaxed and columnar dendrites of Fe–0.82 wt% C alloy simplified from continuously cast SWRH82B steel with forced convection.

2. Model description

Because the nucleation is neglected, governing equations of dendritic growth under forced melt flow include momentum, mass and heat transport equations and the interface evolution equation.

2.1. Transport models

Because of the complex dendritic morphology and its evolution, the inter- and exter-dendritic flows are intricate and give rise to much obstacle in complete and elaborate description of these phenomena. Therefore, some researches [2–6,37] employed the volume averaging approach and Darcy's law to account for the porous property of mushy zone where dendrites grew. In microscopic simulation, especially with CA approach, even simpler assumption that the melt is convective and incompressible Newtonian fluid during dendritic growth was proposed to couple the dendritic evolution directly with melt flow [9,11,13,15,16,18–30,35–36]. The convection flow of the incompressible melt is governed by the continuity and the momentum conservation equations, which are expressed as follows:

Continuity equation:

$$\nabla \cdot (\rho \mathbf{U}) = 0 \quad (1)$$

Momentum conservation equation:

$$\rho \frac{\partial \mathbf{U}}{\partial t} + (\rho \mathbf{U}) \cdot \nabla (\mathbf{U}) = -\nabla p + \nabla \cdot (\mu \nabla (\mathbf{U})) \quad (2)$$

where \mathbf{U} is velocity vector, (u, v) , ρ is density, μ is viscosity, p is the hydrostatic pressure, and t is solidification time. In present work, the densities of liquid and solid phases are separately constant, while densities of the solidification interface cells are interpolated according to their solid fraction, f_s . As dendrites grows, the state of CA cells changes gradually from liquid to interface to solid state, definitely inducing an “isolate island” problem during the calculation of momentum transport problems. However, in order to keep the continuity of discretized momentum equations and ensure the accuracy of solutions, the viscosity of solid dendrites is considered to be much higher than that of liquid phase [41], which keeps constant in this paper.

The solute transport processes in liquid phase and solid phase are considered to be independent, although they are connected by solute redistribution and rejection at solidification interface, as shown in Eq. (3). Therefore, the liquid concentration in liquid phase and interface is determined by both diffusion and convection, while only diffusion for the solid concentration in solid phase and interface. The governing equation of solute transfer under melt flow is expressed as Eq. (4).

$$C_s^* = k_0 C_l^* \quad (3)$$

$$\frac{\partial C}{\partial t} + (\xi \mathbf{U}) \cdot \nabla C = D \cdot \nabla^2 C \quad (4)$$

where C_l^* and C_s^* are equilibrium solute concentration in solid and liquid phase at solidification interface, respectively, k_0 is the equilibrium partition coefficient of solute at solidification interface, ξ is a parameter representing the convection effect, C is solution concentration, and D is diffusion coefficient, which is the function of f_s , solid diffusivity, D_s and liquid diffusivity, D_l under the specific temperature. ξ and C dependent on the CA cell state, are 1 and liquid concentration, C_l , for the diffusion and convection of liquid phase and interface, whereas 0 and solid concentration, C_s , for the diffusion of solid concentration. Moreover, during the calculation of diffusion and convection of liquid phase and interface, solid dendrites are set as isolate islands to avoid the introduction of diffusion from them. However, the diffusion equation of solid phase is explicitly solved.

Additionally, the undercooling as the driving force for dendritic growth is necessary in present work. The melt undercooling dominates the free growth of the equiaxed dendrite, accordingly it is usually assumed to be constant, especially in LGK analytical model. Therefore, the melt undercooling is kept constant through neglecting the heat transfer [19–21,23–28] or dynamically adjusting heat transfer boundaries [14,33,44]. In present work, the former method is employed. However, the growth of columnar dendrites is driven by the dendritic tip undercooling, which is determined by the cooling condition in directional solidification. Therefore, the heat transport is taken into account during the growth of columnar dendrites. The governing equation of heat transfer under melt flow is expressed as Eq. (5).

$$\frac{\partial T}{\partial t} + \mathbf{U} \cdot \nabla T = \alpha \cdot \nabla^2 T + \frac{L}{c} \frac{\partial f_s}{\partial t} \quad (5)$$

$$\alpha = \frac{\lambda}{\rho c} \quad (6)$$

where T is temperature, α is thermal diffusivity of steel, which is the function of the thermal conductivity, λ and the specific heat capacity, c , as expressed in Eq. (6), and L is solidification latent heat of steel. Compared with solute transport, heat transport is successive in the domain regardless of the CA cell state.

Beside the requirement about the conservation of the continuity equation, the convergence of momentum, solute and heat transport equations should satisfy Eqs. (7) and (8):

$$\text{Max} \left[\frac{\zeta_{ij}^{n+1} - \zeta_{ij}^n}{\text{CT}} \right] < \chi \quad (7)$$

$$\text{CT} = \begin{cases} 1 & \zeta_{ij}^0 \geq 1 \\ \zeta_{ij}^0 & \zeta_{ij}^0 < 1 \end{cases} \quad (8)$$

where ζ represents field variables, including u , v , T and C , ζ^0 is on behalf of initial values of these variables, n is iteration steps, χ is a number far less than unity, CT is a constant dependent on ζ^0 , and (i,j) represents the serial number of the CA cell.

2.2. CA model

The CA model is generally characterized by cell geometry, cell state (solid, liquid and interface), neighboring configuration and state transition rulers [32]. Accordingly, the change and the ruler of capturing neighbor cell are the key parts of the dendritic growth model. In this paper, the change of CA cells from liquid state to interface state and from interface state to solid state depends on the Neumann ruler and the solid fraction, respectively. As one CA cell become solid, it will capture liquid cells among its first four nearest neighboring cells as interface cells. The evolution of the interface is controlled by the solute balance at solidification interface, as expressed in Eq. (9) [32–34]. The component of evolution velocity along x axis is shown in Eq. (10) [32], while the form of y component of growth velocity is similar.

$$v_n C_l^* (1 - k_0) = D_s \frac{\partial C_s}{\partial n} \Big|_* - D_l \frac{\partial C_l}{\partial n} \Big|_* \quad (9)$$

$$v_x(i,j) = \frac{1}{\Delta x(1-k_0)C_l^*(i,j)} \{ D_s [(C_s^*(i,j) - C_s(i-1,j))f_s(i-1,j) + (C_s^*(i,j) - C_s(i+1,j))f_s(i+1,j)] + D_l [(C_l^*(i,j) - C_l(i-1,j))(1-f_s(i-1,j)) + (C_l^*(i,j) - C_l(i+1,j))(1-f_s(i+1,j))] \} \quad (10)$$

where v_n and v_x are normal and x component of growth velocity of solidification interface, respectively. The equilibrium solute concentration in liquid phase at solidification interface, C_l^* is the function of equilibrium temperature, T^* , average curvature, $\bar{\kappa}$ and anisotropy of surface tension, $f(\varphi, \theta)$ of solidification interface, as shown in Eq. (11) [14,18,27,29–39].

$$C_l^* = C_0 + \frac{1}{m_l} (T^* - T_l + \Gamma \bar{\kappa} f(\varphi, \theta)) \quad (11)$$

where C_0 is initial content of solute in the modeling domain, T_l is equilibrium liquidus temperature, m_l is the slope of liquidus line in Fe-C equilibrium phase diagram, and Γ is the Gibbs-Thomson coefficient of Fe-C alloy. T^* is determined according to the preset melt undercooling for equiaxed dendrites and from the results of heat transfer calculation for columnar dendrites, respectively. $\bar{\kappa}$ is calculated according to the normal gradient of solid fraction at solidification interface, as expressed in Eq. (12). $f(\varphi, \theta)$ is the function of the normal direction of solidification interface and the preferential growth direction, as shown in Eqs. (13) and (14) [14,30,31,33–35].

$$\bar{\kappa} = \frac{2(f_s)_x(f_s)_y(f_s)_{xy} - (f_s)_x^2(f_s)_{yy} - (f_s)_y^2(f_s)_{xx}}{[(f_s)_x^2 + (f_s)_y^2]^{3/2}} \quad (12)$$

$$f(\varphi, \theta) = 1 - 15\epsilon \cos(4(\varphi - \theta)) \quad (13)$$

$$\varphi = \arccos \left(-\frac{(f_s)_x}{[(f_s)_x^2 + (f_s)_y^2]^{1/2}} \right) \quad (14)$$

where $(f_s)_x$ and $(f_s)_y$ are first order derivatives of solid fraction, $(f_s)_{xx}$, $(f_s)_{xy}$ and $(f_s)_{yy}$ are second order derivatives of solid fraction, ϵ is the parameter for anisotropy of surface tension, and φ and θ are angles of the normal direction of solidification interface and the preferential growth direction with respect to x axis, respectively.

In present work, the solidification interface is assumed to be planar, therefore the increment of solid fraction, Δf_s is predicted according to components of the interface velocity. Then the solid fraction of solidification interface cell is updated, as well as the normal growth velocity, v_n . The related equations are listed in Eqs. (15)–(17) [32,33].

$$\Delta f_s = \frac{\Delta t}{\Delta x} \left(v_x + v_y - v_x v_y \frac{\Delta t}{\Delta x} \right) \quad (15)$$

$$f_s^{t+\Delta t} = f_s^t + \Delta f_s \quad (16)$$

$$v_n = \Delta f_s \frac{\Delta x}{\Delta t} \quad (17)$$

where Δt is time step, and Δx is CA cell size.

With the growth of dendrites, solute concentration in liquid phase increases gradually in the interface cell and discharges to its neighboring liquid as the concentration is higher than the equilibrium concentration at the interface. As the solid fraction of solidification interface cell is greater than unity, it becomes solid and captures the first four nearest neighbor cells as interface cells. Simultaneously, the solute in residual liquid phase discharges to its neighboring liquid due to the complete solidification. The discharging amount from interface cell to its neighbors depends on the solute concentration difference between them.

Because the solidification interface and the solute diffusion in solid phase are explicitly tracked and calculated, the time step will be controlled by interface evolution and solute diffusion in solid phase.

$$\Delta t \leq \min \left[\frac{\Delta x}{v_{n,\max}}, \frac{(\Delta x)^2}{4D} \right] \quad (18)$$

where $v_{n,\max}$ is the maximum growth velocity of solidification interface at time t .

3. Mathematical tests

The initial value of temperature within the modeling domain is equilibrium liquidus temperature, T_l , of Fe-0.82 wt% C alloy for columnar dendritic growth and temperature with a certain undercooling, ΔT , below T_l for equiaxed dendritic growth. In addition, the entire modeling domain is in liquid state with initial concentration C_0 before the solidification is ignited. Several nuclei are artificially placed in the domain for the simulation of both equiaxed dendrites and columnar dendrites. The equilibrium liquidus temperature is calculated according to the melt temperature of pure iron, T_m , and the slope of liquidus line, m_l , in Fe-C binary phase diagram. The related parameters for solving transport and growth kinetics equations are listed in Table 1 [32,43–48].

In order to investigate equiaxed and columnar dendritic growth under forced melt flow, four flow patterns with different flow boundaries are designed. In present work, non-slip boundary conditions are set at walls and solid islands such as balls and columns, while the symmetry and the well developed outflow are established at symmetrical boundaries and outlets [41]. Accordingly, velocities at outlets are modified with consideration of mass conservation. In present work, equiaxed dendrites are assumed to grow in melt with constant undercooling, and thus the heat transfer is neglected. The effect of melt flow on equiaxed dendritic growth is conveyed mainly through its influence on

Table 1

Related physical property parameters for transport phenomena and growth kinetics [32,43–48].

| Parameters for heat transport | | | Parameters for solute and momentum transport | | | |
|----------------------------------|-----------|--------------------|--|---------------|---|--|
| Melt temperature, K | T_m | 1809 | Liquidus line slope, K/wt% | m_l | −78.0 | |
| Conductivity, W/(m K) | λ | 33.0 | Diffusion coefficient, m ² /s | D_s | $7.61 \times 10^{-6} \exp(-134,564/RT)$ | |
| Density, kg/m ³ | ρ_s | 7400 | | D_l | $7.67 \times 10^{-6} \exp(-106,000/RT)$ | |
| Specific heat capacity, J/(kg K) | ρ_l | 7020 | Gas constant, J/(K mol) | R | 8.314 | |
| | c_s | 648 | Partition coefficient | k_0 | 0.34 | |
| | c_l | 824 | Parameter for anisotropy | ε | 0.04 | |
| | c_m | 770 | Gibbs–Thomson coefficient, K m | Γ | 1.9×10^{-7} | |
| Latent heat, J/kg | L | 2.72×10^5 | Viscosity, kg/(m s) | μ | 5.5×10^{-3} | |

solute distribution. As columnar dendrites generally grow anti-parallel to the direction of heat flux in directional solidification of alloys, a similar condition is artificially designed. The heat is extracted only from the bottom of the modeling domain during the growth of columnar dendrites in this paper. It should be stated that only the effect of melt flow on solute and temperature distribution in the modeling domain, especially around solid dendrites are concerned by researches to investigate its influence on dendritic morphology in microscopic simulation, although this assumption is very idealistic [19–28,30,35–36,39]. Therefore, regardless of flow pattern and dendrite type, the solute flux at boundaries of modeling domain is supposed to be zero to avoid introducing additional solute and heat by the melt fluid into the modeling domain where dendrites grow. Mathematical tests about the capacity of the CA model for dendritic growth, the momentum model and the heat transfer model are carried out within the modeling domain as the same as those used in the simulation of dendritic growth under melt flow and through comparing with results from LGK analytical model, FLUENT 12.0 and ANSYS 12.0 (Ansys Inc., Canonsburg, PA). It should be mentioned that these tests give an indirect validation of the present self-developed codes because of the huge obstacle to direct validation by commercial software, such as different meshing requirements and approaches, especially in irregular domains, and inflexible dealing with interface evolution and solute diffusion of different phases. The concept of indirect validation can be seen in the work of Yin et al. [30], although the validity of the velocity field is not mentioned in that work.

3.1. CA model

The predicted dendritic morphology varies a lot because of different alloy systems and considerations in models, however the steady growth velocity of dendritic tip is mainly concerned to evaluate the model capacity through the comparison with the LGK analytical model and investigate the effect of the melt flow [14,19–21,23–28,30,33–37,39,44]. In present work, a 200 μm × 200 μm modeling domain is discretized into 201 × 201 CA cells. A single nucleus with the preferred orientation in accordance with grid is placed in the center of the domain and grows at the preset melt undercooling from 3 K to 10 K. The average interface advancing velocity, \bar{v}_n defined according to CA cell size and its residual time in the interface state, is used to determine tip growth velocities of equiaxed dendrites. Fig. 1(a) shows the variation of average growth velocity of dendritic tip with the solidification proceeding at 6 K undercooling. The equiaxed dendrite firstly undergoes a transient and then a gentle period, during which the average velocity of the dendritic tip keeps decreasing. Therefore, it is difficult to evaluate steady growth velocities of equiaxed dendritic tips. According to Beltran-sanchez and Stefanescu [33], as the solute concentration at the modeling domain wall opposite to the dendritic tip reaches 1.01 times of initial concentration, the equiaxed dendrite moves into steady growth, and thus the steady growth

velocity of dendritic tip is determined. Accordingly, the equiaxed dendrite of Fe–0.82 wt% C alloy will reach steady state in 288.4 ms after nucleation at 6 K melt undercooling. Moreover, the calculated steady growth velocity is 130 μm/s, which agrees well with 137 μm/s predicted by LGK analytical model, as shown in Fig. 1(a). Fig. 1(b) shows the comparison of the steady growth velocities of dendritic tip of Fe–0.82 wt% C alloy calculated from the CA model and those determined from LGK analytical model at different melt undercoolings. The results from the CA model agree well with those from LGK analytical model within 5–7 K undercooling. The deviation between them increases as the undercooling moves further than 6 K, although it is negative above 6 K and positive below 6 K. The variation tendency is consistent with that of Fe–0.6 wt% C alloy predicted by Li et al. [37], however contrary to that of Fe–0.6 wt% C alloy predicted by Beltran-sanchez and Stefanescu [33]. In the following calculation, the CA cell size is about 1.0 μm except for being specially mentioned. Dendrites of high carbon Fe–C alloy grow slowly because of the low diffusion coefficient, indicating enough time and space in the designed domain to investigate the effect of melt flow on dendritic morphology, especially lengths of dendritic arms.

3.2. Transport models

In order to ensure the accuracy of self-developed codes in solving momentum and heat transport problems during dendritic growth, similar situations were designed. Flows around a solid ball and solid columns were concerned for equiaxed and columnar dendrites, respectively. Additionally, heat losses during the directional solidification were interested.

3.2.1. Models for equiaxed dendrites

A solid ball with a radius of 30 μm is placed in the center of the modeling domain which is as the same as that for equiaxed dendrites, as well as the discrete approach. The molten steel flows into the domain from the left boundary and leaves with a full development at the right boundary, while other boundaries are regarded as symmetry, which is noted as Case I. In Case II, the molten steel flows into the domain from left and top boundaries and leaves with full developments at right and bottom boundaries. The inlet velocity varies from 0.001 m/s to 0.005 m/s with a step of 0.002 m/s. The velocity vectors at outlets of both cases are schematically shown in Fig. 2. After the flow reaches steady state, velocity fields represented by horizontal velocities in vertical symmetrical line are extracted to compare with the results from FLUENT 12.0.

Fig. 3 shows the comparison of monitored horizontal velocities calculated by self-developed codes and FLUENT 12.0 under two different flow patterns. The results of present model are well consistent with those of FLUENT 12.0 as the inlet velocity varies from 0.001 m/s to 0.005 m/s, especially near the solid ball. It should be mentioned that absolute criterion both for the residual of horizontal and vertical velocities is 1.0×10^{-3} during the calculation of FLUENT 12.0 in present work, while those of continuity

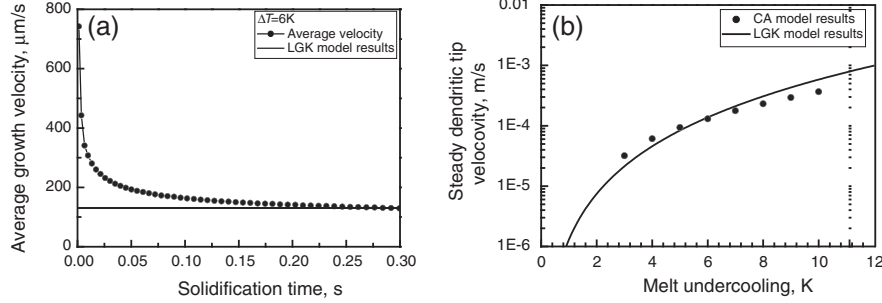


Fig. 1. (a) Average growth velocities at 6 K undercooling and (b) comparison of steady growth velocities of equiaxed dendritic tip from the CA model and LGK model.

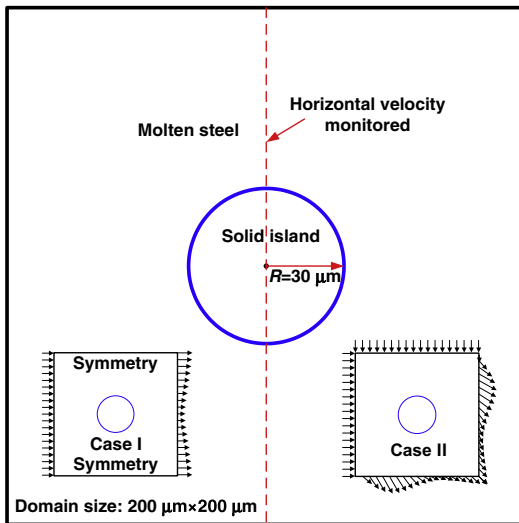


Fig. 2. Design of flow around a solid ball and velocity vectors in two different cases.

are 1.5×10^{-3} and 3×10^{-4} in Case I and Case II, respectively. Therefore, the present self-developed codes exhibit a better performance in Case II.

3.2.2. Models for columnar dendrites

For columnar dendrites, a $204\text{ }\mu\text{m} \times 612\text{ }\mu\text{m}$ modeling domain with 204×612 cells is designed. Four nuclei are placed at the bottom of the domain with the same interval of $51\text{ }\mu\text{m}$. A directional solidification situation is created, so that the heat is only extracted from the domain bottom. During the growth of columnar dendrites, a fluid with a preset velocity flows into the domain at left side and out from the right side with well development, which is noted as Case III. The bottom and top sides of the domain are supposed to be a wall and symmetrical, respectively. A similar

situation for investigating the capacity of present self-developed codes in describing the flow over solid columns is designed as shown in Fig. 4(a), as well as the boundary conditions for flow and heat transfer calculation in Fig. 4(b) and (c). It should be noted that the domain sizes and designs in Fig. 4(a)–(c) are the same, although Fig. 4(b) and (c) are visually shrunk to compact the figure space. The flow of the melt and its heat transfer are solved separately as the former one is a steady state problem, while the latter one is a transient one. However, during the calculation of columnar dendritic growth under melt flow, both of them are transient, and the heat transport is solved after the flow equations reaches convergence, as well as the solute transport. The horizontal velocities and temperature distribution in vertical symmetrical line are concerned as the flow calculation is converged and heat transfer undergoes 0.1 ms with a time step of 0.01 ms, which are shown in Fig. 4(d) and (e). Both flow and heat transfer results agree well with those of FLUENT 12.0 and ANSYS 12.0 under different inlet velocities and heat fluxes. The absolute criteria for the residual of horizontal and vertical velocities and continuity are set to be 1.0×10^{-3} , 1.0×10^{-3} and 7.0×10^{-4} in FLUENT calculation. In addition, the tolerance for ANSYS 12.0 is set to be 1.0×10^{-4} in L2 norm, however it is much lower than the preset values when the convergence is reached.

Additionally, in order to investigate the effect of circular flow on columnar dendritic growth, the molten steel flowing into a $408\text{ }\mu\text{m} \times 408\text{ }\mu\text{m}$ domain with 408×408 cells from the left boundary is turned to vertical direction and leaves from the top boundary with full development. Eight nuclei with the same arrangement as that in Case III are placed in bottom and right walls respectively, and grow up as the heat is extracted there, which is regarded as Case IV. A similar design that nuclei are substituted with $23.5\text{ }\mu\text{m}$ height columns is carried out as shown in Fig. 5(a). The horizontal velocities in vertical symmetrical line agree well with the results of FLUENT 12.0 under different inlet velocities, as shown in Fig. 5(b). The absolute criteria of horizontal and vertical velocity residuals are as the same as those in aforementioned cases, however the residual of continuity reduces to

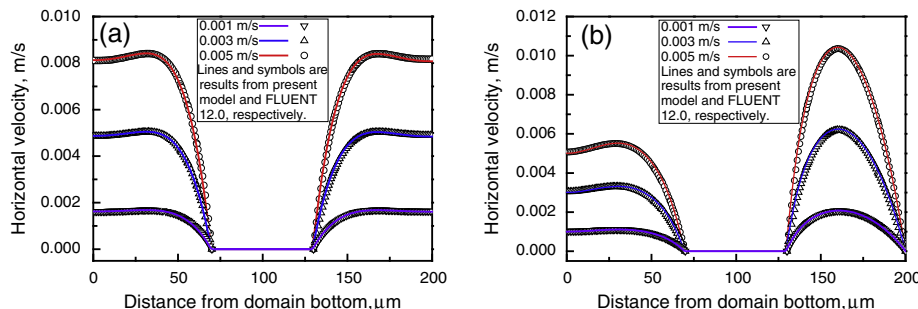


Fig. 3. Comparison of monitored horizontal velocities calculated by self developed codes and FLUENT 12.0, (a) Case I and (b) Case II.

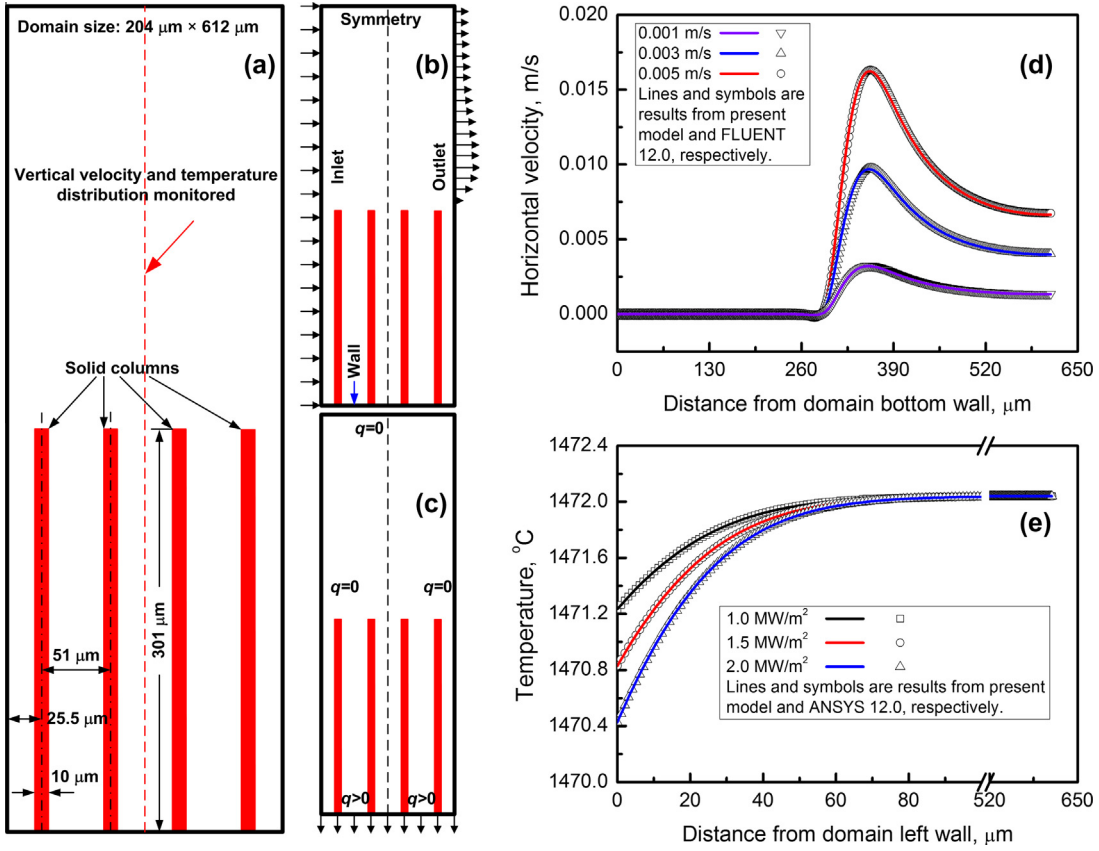


Fig. 4. Design of the left-in and right-out flow over solid columns in the directional solidification and comparison of results between the present model and commercial software: (a) design schematic, (b) flow boundaries, (c) thermal boundaries, (d) monitored horizontal velocities and (e) monitored temperature distribution. Note: the domain designs and sizes of (a–c) are the same, although (b) and (c) are visually shrunk to make the figure compact.

8.0×10^{-5} in FLUENT calculation. As the iteration is converged, residuals of horizontal and vertical velocities are further lower than preset criteria in such four cases.

4. Results and discussion

Based on results from aforementioned mathematical tests, the self-developed codes are used to investigate the effect of melt flow on equiaxed dendrite and columnar dendritic growth. Beside the inlet velocity, the melt undercooling and the flow pattern are taken into account in Case I and II for equiaxed dendrites, as well as the heat flux in Case III and IV for columnar dendrites.

4.1. Equiaxed dendrites

Firstly, the growth of a single equiaxed dendrite in Case I is discussed. In present paper, left, right, top and bottom arms of an equiaxed dendrite are noted as L, R, T and B, respectively. The morphology and solute distribution of an equiaxed dendrite are presented after 200 ms at undercooling 5 K and 55 ms at undercooling 15 K, with inlet velocity varying from 0.001 m/s to 0.005 m/s, as shown in Fig. 6. As the melt flow is introduced, the four fold symmetry of an equiaxed dendrite is destroyed, and changes into symmetry in horizontal direction, since the left (upstream) arm is promoted and the right (downstream) arm is restrained. It is

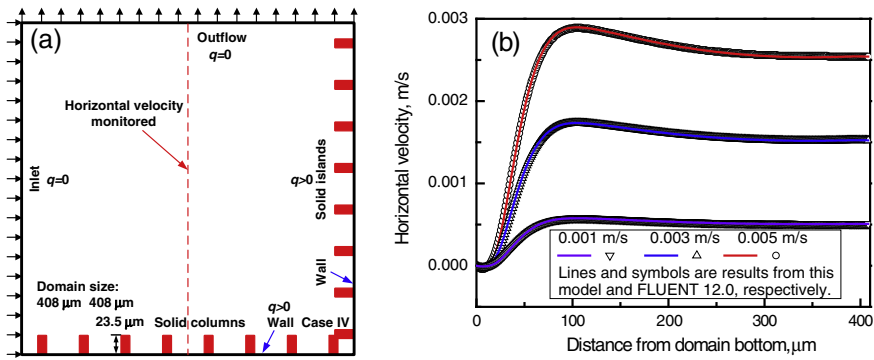


Fig. 5. Design of the left-in and top-out flow over solid columns and comparison of results between the present model and FLUENT 12.0: (a) design schematic, (b) monitored horizontal velocities.

mainly ascribed to that the solute enriched around dendritic tips at left, top and bottom sides due to the evolution of solidification interface will be carried away by melt flow and gather around the right arm as the fluid gets over top and bottom arms and flows down to the right arm, as shown in Fig. 6. If there is no special statement, one velocity vector is plotted in every $6.0 \mu\text{m} \times 6.0 \mu\text{m}$ CA cell for a clearer visualization. The solute enriched layer at left tip, top and bottom tips and right tip will get much thinner, thinner and much thicker, respectively, compared with the situation without melt flow. Therefore, left, top and bottom arms get fatter and longer, while right arm becomes thinner and shorter, especially at the lower melt undercooling.

The relative deviation, Rd_i , between dendritic arm lengths under melt flow and without flow defined as Eq. (19) is used to investigate the effect of melt flow.

$$Rd_i = \frac{l_{ij} - l_{i,0}}{l_{i,0}} \times 100\% \quad (19)$$

where l_{ij} is the arm length of the equiaxed dendrite, i represents the arm index among L, T, R and B, and j represents the case index and 0 is for the case without melt flow, 1 for Case I and 2 for Case II. Fig. 7 shows the values of Rd_i under the conditions as the same as those in Fig. 6. As inlet velocity increases, the solute in upstream side is more easily blown to the downstream side, which causes the solute layer at the downstream side to be thicker and sharper. Therefore, the phenomenon of promoted growth at the upstream side is aggravated with the increase of inlet velocity, as shown in Figs. 6 and 7. At a lower melt undercooling, the morphology of the equiaxed dendrite is more asymmetrical because the solute gradient in front of the downstream tip reaches saturation more easily compared with the situations at a deeper melt undercooling.

In order to investigate the growth behavior of equiaxed dendrite in Case II and its comparison with that in Case I, dendritic tip velocities are recorded till it undergoes 30 CA cells at 5 K undercooling and inlet velocity of 0.001 m/s, as well as the dendritic morphology and velocity vectors as the right tip reaches the 30th CA cell at 282.5 ms, as shown in Fig. 8. In Case II, the melt flows into the modeling domain from left and top boundaries in an

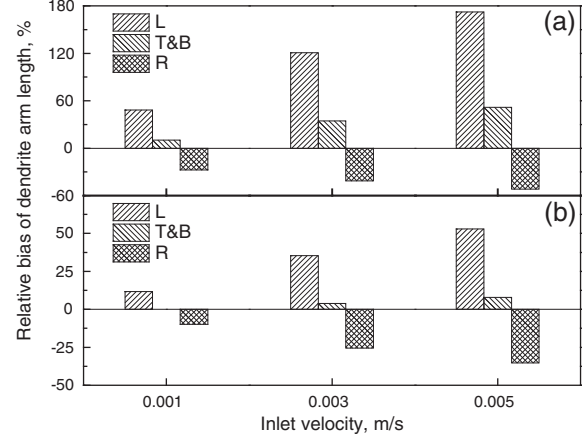


Fig. 7. The relative deviation between dendritic arm lengths with flow of Case I and those without flow at melt undercooling (a) 5 K and (b) 15 K.

orthogonal direction and interacts to form a symmetrical flow field along the domain diagonal. As the top and the left arms grow up, the flow near the domain diagonal will be hindered and turns to get over arms, causing two symmetrical vortexes near the dendrite neck, as shown in Fig. 8(a). The solute enriched near those arms is carried away, so that their growth is facilitated. Moreover, the left tip in Case II grows significantly faster than that in Case I due to a greater velocity magnitude, as shown in Fig. 8(b). After the melt gets over the top tip, it immediately turns down under the effect of vertical flow, which causes a tiny vortex near the dendrite neck, as shown in Fig. 8(a). As the melt collides with the right arm, it turns again to climb over the right arm. The growth of the right tip is constrained due to the solute enrichment caused mainly by melt flow. However, the enriched solute is more easily carried away by the oblique flow than the horizontal flow in Case I, which gives rise to a faster growth velocity, as shown in Fig. 8(b). Meanwhile, two symmetrical vortexes form between the right and the bottom arms, as shown in Fig. 8(a). The differences of growth velocities between Case II and Case I become more and more

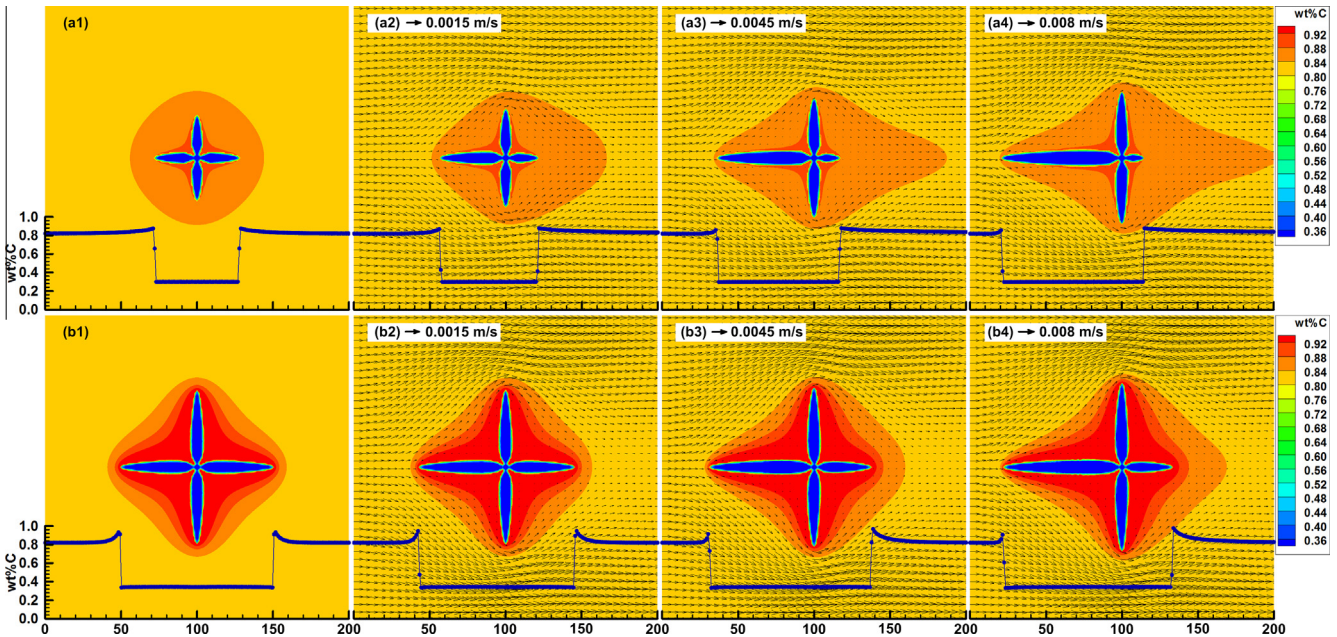


Fig. 6. The morphology and solute distribution during equiaxed dendritic growth at melt undercooling of (a) 5 K after 200 ms and (b) 15 K after 55 ms with the inlet velocity (1) 0, (2) 0.001 m/s, (3) 0.003 m/s and (4) 0.005 m/s in Case I.

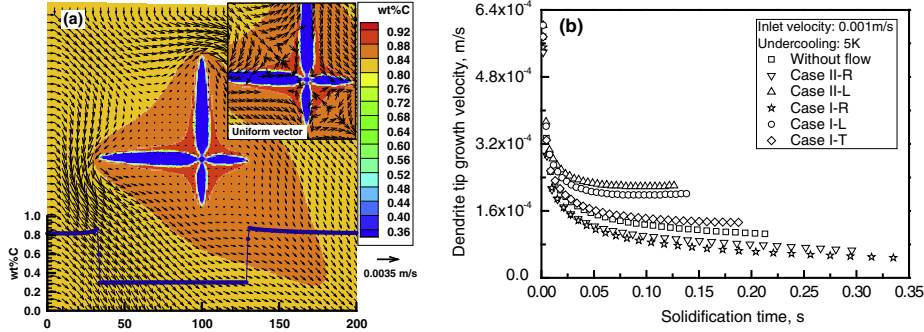


Fig. 8. Comparison of dendritic growth between Case I and Case II at 5 K undercooling and inlet velocity of 0.001 m/s: (a) dendritic morphology and velocity vector after 282.5 ms of Case II and (b) dendritic tip velocities.

significant after the transient growth period with the solidification proceeding, indicating the effect of melt flow is relatively strengthened.

Fig. 9 shows the values of Rd_i in Case II with solidification times and melt undercoolings as the same as those in Case I in Fig. 7, as the inlet velocity changes from 0.001 m/s to 0.005 m/s. Both in Case I and Case II, the growth of left arms presents similar tendencies with the variation of inlet velocity and melt undercooling, as shown in Figs. 7 and 9. However, with the introduction of inlet flow from top boundary, the flow near left and top tips is intensified, so that left and top arms grow faster compared with those in Case I. Accordingly, the effect of inlet flow velocity and melt undercooling on them is manifested. At deep melt undercooling, the inhibited growth of right arms is intensified with the increase of inlet velocity, however it becomes more serious than that in Case I with low inlet velocity and less serious with high inlet velocity, as shown in Figs. 7(b) and 9(b). The severer inhibition with low inlet velocity can be interpreted by the intensified flow of Case II. It indicates that the oblique flow near the right tip alleviates the solute enrichment due to melt flow to some extent and its effect improves with the increase of inlet velocity, which can also be deduced from much lower increments of the relative deviation than those in Case I, as shown in Fig. 9(b). At lower melt undercooling, the interaction of solute enrichment and the oblique flow near the right tip keeps a relative steady state, while the effect of oblique flow improves slightly with a higher inlet velocity, as shown in Fig. 9(a). Moreover, the relative deviation of right arms in Case II are completely lower than those in Case

I. Therefore, the effect of oblique flow becomes more significant at the lower melt undercooling.

The promotion of the development of secondary dendrite arms due to melt flow is not observed in both Case I and Case II. On the one hand, it is mainly ascribed to the small domain size and the neglect of heat transfer. On the other hand, it is because the relatively lower melt undercooling of high carbon Fe-C alloy in the present work. The phenomenon will be described in detail in future work about dendritic growth of low carbon Fe-C alloy and low carbon steel with relatively deeper melt undercooling due to a higher diffusion coefficient and a lower equilibrium partition coefficient at the solidification interface.

4.2. Columnar dendrites

Fig. 10 shows morphology and solute distribution of columnar dendrites under heat flux of 1.5 MW/m^2 as the inlet velocity varies from 0 to 0.005 m/s in Case III. In order to investigate the initial evolution of columnar dendrite under melt flow, bottom parts with columnar dendrites were captured from the entire domain at different solidification time. Fig. 11 shows the growth process of columnar dendrites with heat flux of 1.5 MW/m^2 and inlet velocity of 0.003 m/s. The vector is plotted in Fig. 11(a) with 8 nodes skipped in both horizontal and vertical directions. Moreover, Fig. 11 can be correctly read according to the reference scale. As the solute and the heat brought in and carried out by melt fluid are neglected, the solute concentration and the temperature at the inlet and the outlet change with those of internal cells, as shown in Figs. 10 and 11. Columnar dendrites in the domain are in sequence noted as A, B, C and D from left to right. Without the melt flow, each columnar dendrite in the domain develops a similar and symmetrical morphology. With the solidification proceeding, the solute inevitably enriches more and more at columnar dendrite roots and less at tips, causing a layered distribution pattern. As the melt flow is introduced, the solute enriched at the root of columnar dendrite A is blown up, accordingly the growth of A is the first to be inhibited. Subsequently, the melt with enriched solute will flow to next columnar dendrites and inhibit their growth successively, as shown in Fig. 11. Generally, the growth of columnar dendrites is inhibited under melt flow of Case III, especially with higher inlet velocities, as shown in Fig. 10. However, as the inlet velocity is 0.001 m/s, the solute enriched melt cannot be transported to the downstream side in time, on the other hand, the solute enriched near tips of C and D due to solute rejection is carried away by melt flow, and thus their growth is promoted. Moreover, the melt flow disturbs the solute distribution and causes the asymmetry of columnar dendrites. As the growth is inhibited, primary and secondary dendrite arms become fatter compared with those without melt flow. It is observed that secondary

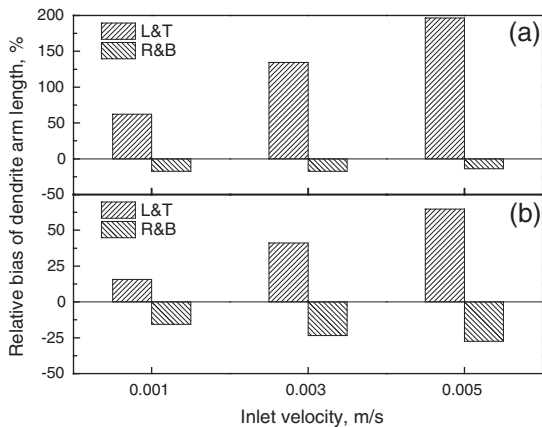


Fig. 9. The relative deviation between dendritic arm lengths with flow of Case II and those without flow at melt undercooling (a) 5 K and (b) 15 K.

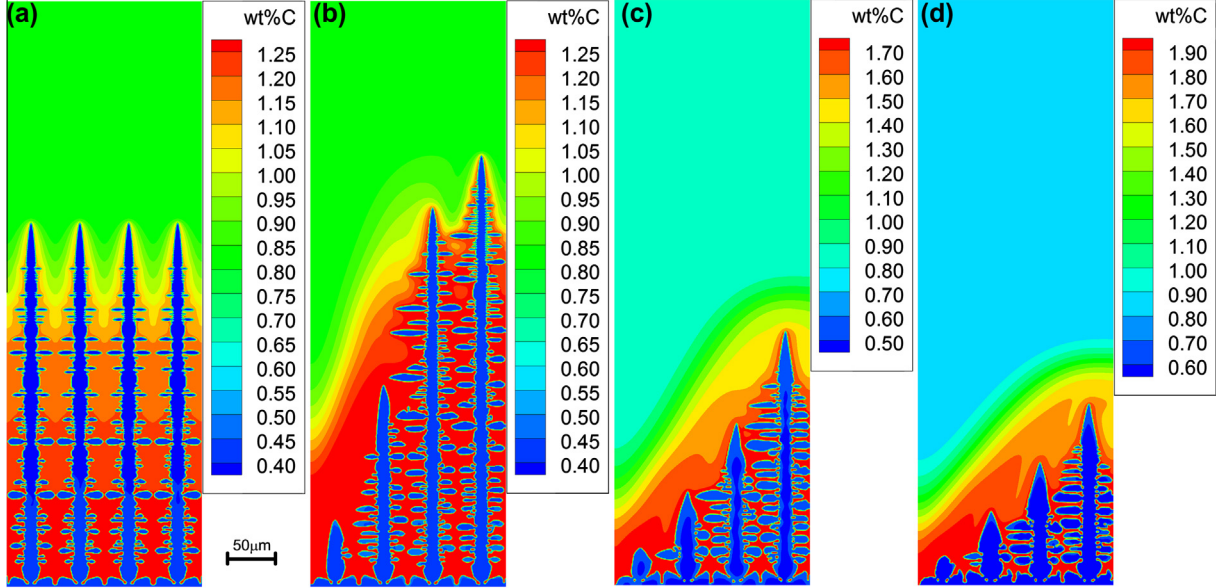


Fig. 10. Columnar dendrites after 225 ms under heat flux of 1.5 MW/m^2 with inlet velocity of (a) 0, (b) 0.001 m/s , (c) 0.003 m/s and (d) 0.005 m/s .

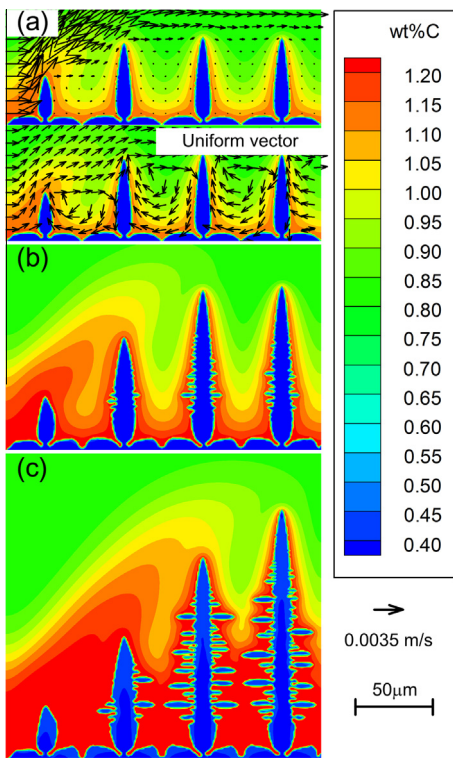


Fig. 11. Morphology of columnar dendrites with heat flux of 1.5 MW/m^2 and inlet velocity of 0.003 m/s after (a) 52.5 ms, (b) 77.5 ms and (c) 102.5 ms.

dendrite arms starts to form in primary branches at the downstream side and are better developed at left sides at initial solidification stage, as shown in Fig. 11(b). Zhu et al. [21] exerted a flow field entering at left side and leaving from right side on the columnar dendritic growth and found that secondary dendrite arms at left side of the primary branches were more developed than those at the right side. Yuan and Lee [39] introduced nature convection with a 30° angle deviating from the horizontal plane into the columnar dendritic growth and found the development of secondary dendrite arms at the right side of the primary branches was

promoted. Although those phenomena are quite different, they contain the similar mechanism, that is, the effect of melt flow on solute distribution around columnar dendrites. In present work and that of Zhu et al. [21], the melt flow starting from left boundary preferentially collides with the left sides of primary branches, turns down, washes them and carries fresh solute down, causing solute disturbance there. In the work of Yuan and Lee [39], the inclined flow is stronger around right sides of primary branches than that around left sides, giving rise to more solute disturbance and development of secondary dendrite arms. With the solidification proceeding, since columnar dendrites interact with each other, right sides of columnar dendrites in the middle (B and C) get much disturbance and form well developed secondary dendrite arms, as shown in Fig. 11(c). However, those secondary dendrite arms at the right side will be inhibited by those at the left side of adjacent columnar dendrites, as shown in Fig. 10(b)–(d). As columnar dendrite A is enveloped with highly enriched solute, it is difficult to develop secondary dendrite arms, especially with higher inlet velocity, as shown in Figs. 10 and 11.

With the increase of heat flux, columnar dendrites grow faster and form more developed and fatter secondary dendrite arms, especially those of the columnar dendrite B, improving the compactness in the domain, as shown in Fig. 12. Moreover, under higher cooling intensity, columnar dendrites at the downstream side gradually break through the blockade of solute enriched layer induced by melt flow and become significantly higher than those in the upstream side, as shown in Fig. 12(b) and (c). Therefore, the inhibition effect of melt flow on dendrites is more significant under lower cooling intensity.

In order to investigate the influence of columnar dendritic growth and melt flow on temperature distribution and temperature variation on dendritic growth, the temperature distribution without and with dendritic growth and melt flow at the same solidification time and cooling condition as those in Fig. 11 is presented in Fig. 13. As the dendritic growth is introduced, the release of solidification latent heat improves the temperature in the domain and causes some fluctuations near the tips of columnar dendrites, as shown in Fig. 13(a) and (d). As the melt flow is taken into consideration, the growth of columnar dendrites is generally inhibited, reducing latent heat released and temperature in the domain, as shown in Fig. 13(b)–(d). Under low flow intensity

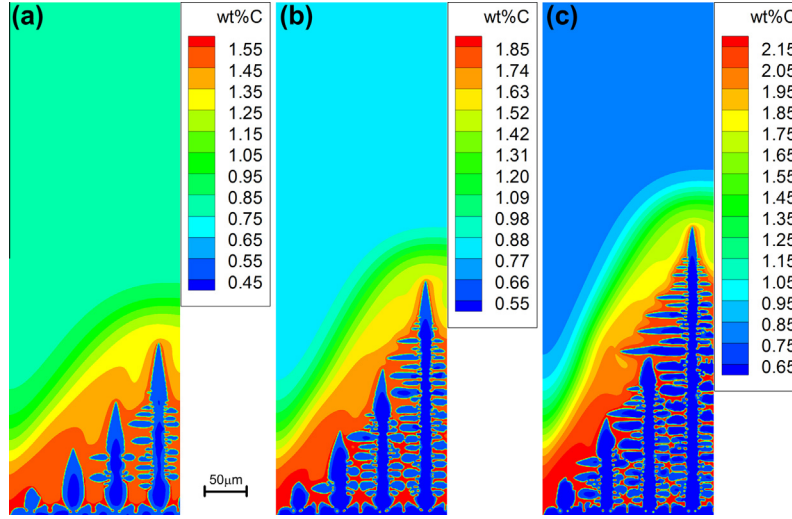


Fig. 12. Morphology of columnar dendrites after 250 ms with inlet velocity of 0.003 m/s as the heat flux is (a) 1.0 MW/m², (b) 1.5 MW/m² and (c) 2.0 MW/m².

conditions, the growth of columnar dendrites at the downstream side is promoted, which gives rise to a higher temperature near their tips, as shown in Figs. 10(b) and 13(c). Although deeper melt undercooling is generated with the increase of flow intensity, the high concentrated solute at dendritic tips caused by melt flow will inhibit their growth. Consequently, the effect of melt flow on solute distribution dominates the columnar dendritic growth under melt flow, which is similar with the assumption of solute controlled dendritic growth.

Fig. 14 shows morphology of columnar dendrites after 100 ms with heat flux of 1.5 MW/m² under circular flow in Case IV as the inlet velocity varies from 0 to 0.005 m/s, as well as velocity vectors with 10 nodes skipped in both horizontal and vertical directions. Without melt flow, columnar dendrites placed at bottom and right walls grow symmetrically and meet at the domain diagonal, as shown in Fig. 14(a). Additionally, columnar dendrites in the bottom and right corner grow faster than those in the left and the right due to the heat transfer in two dimensions in the corner. As the circular melt flow is introduced, columnar dendrites in the bottom and left corner are inhibited, while those near the

diagonal and near the top outlet are promoted, as shown in Fig. 14(b). It is mainly ascribed to that solute enriched melt is only carried over two columnar dendrites under low inlet velocity, on the other hand solute enriched at other dendritic tips is carried away with the circular flow. With the increase of inlet velocity, the inhibition of columnar dendrites spreads to the third one in the bottom and left corner. The growth of columnar dendrite located at the outlet gets more promotion. Moreover, the next two dendrites are promoted more than those symmetrically in the middle of right wall, as shown in Fig. 14(b). Such phenomena are more aggravated as the inlet velocity rises to 0.005 m/s. Additionally, the columnar dendrite near the middle at bottom wall grows slower than the symmetrical one in the right wall under strong melt flow.

As described above, the melt flow promotes the growth of upstream primary branches of equiaxed dendrites, however inhibits the development of primary branches of columnar dendrites in upstream sides. Although the melt flow causes quite different influence on the growth of equiaxed and columnar dendrites, the same mechanism is well presented. As the dendritic growth is

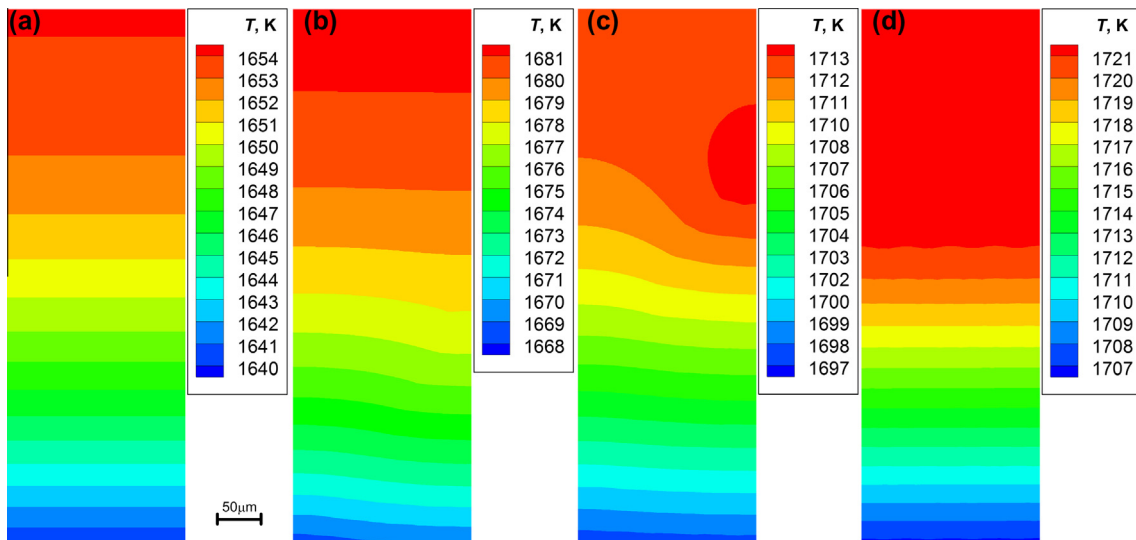


Fig. 13. Temperature distribution after 225 ms under heat flux of 1.5 MW/m², (a) without and with columnar dendrites as inlet velocity is (b) 0.003 m/s, (c) 0.001 m/s and (d) 0 m/s.

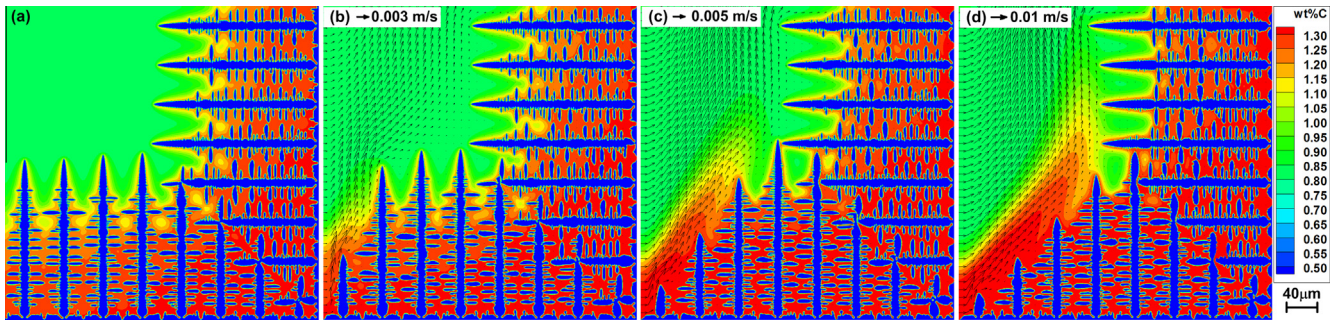


Fig. 14. Morphology of columnar dendrites after 100 ms with heat flux of 1.5 MW/m^2 in Case IV as the inlet velocity is (a) 0, (b) 0.001 m/s, (c) 0.003 m/s and (d) 0.005 m/s.

controlled by solute diffusion, the melt flow influences the dendritic growth mainly through its disturbance on solute distribution around solid dendrites. For equiaxed dendrites, the melt flow easily blows away the solute enriched at dendritic tips at the upstream side and causes solute to gather at the downstream side, and thus promotes the growth at the upstream side and inhibits the growth at the downstream side. For columnar dendrites, the forced flow tends to carry the solute enriched at the roots of upstream columnar dendrites to their tips and inhibits their growth.

During the practical solidification process of alloys, the dendrites nucleate randomly near the mold due to the initial intensive cooling condition and compete with each other according to the direction of heat flow and melt flow. Columnar dendrites whose crystal orientations are parallel to the heat flow direction or toward the upstream direction of the melt flow will win the competition. Therefore, it is usually observed that the columnar dendrites deviate from lines perpendicular to surface and grow toward the flow direction in transverse section of steel blooms and billets by continuous casting, due to the rotation stirring flow field generated by the application of EMS apparatus [49]. However, according to the mechanism of Neumann ruler, the solidification of one CA cell will definitely trigger liquid cells among its first four nearest neighboring cells to become interface state. This mechanism will inevitably cause dendritic branches to grow oriented or at 45° with CA mesh and are with thin and long primary tips [33,34]. Therefore, because of the limitation of present CA model, the deviation of primary branches from the vertical line cannot be revealed in present work, as well as the preferential competition caused by melt flow. In order to simulate the dendritic growth more realistically during the solidification of continuously cast steel, a modified decentered square algorithm which takes the competition and preferential growth of steel dendrites into consideration has been developed and will be reported in the near future.

5. Conclusion

A 2D CA-FVM model with the couple of CA model based on the Neumann capture ruler and transport models in the microscopic scale was developed to investigate dendritic growth of Fe-0.82 wt% alloy under forced melt flow. Moreover, transport models were discretized in the staggered grids and solved with SIMPLE algorithm and block-corrected TDMA method. The capacity of present self-developed codes was evaluated thorough comparison with the results of LGK analytical model and commercial software under four cases designed for equiaxed and columnar dendrites. Subsequently, the growth of equiaxed and columnar dendrites under melt flow in designed cases was discussed in detail. The main conclusions are summarized as follows.

- (1) The CA model presents a good performance in simulating the equiaxed dendritic growth at 5–7 K undercooling. Flow fields calculated by present self-developed codes agree well

with results from FLUENT 12.0 under such four cases, as the inlet velocity varies from 0.001 m/s to 0.005 m/s. Meanwhile, the temperature form the present model shows a good agreement with the prediction of ANSYS 12.0 in Case III, as the heat flux at domain bottom changes from 1.0 MW/m^2 to 2.0 MW/m^2 .

- (2) The growth of equiaxed dendritic arms at the upstream side is promoted, while that at the downstream side is inhibited, because the solute is carried away from the upstream side by the melt flow and enriches at the downstream side. The asymmetrical growth is reinforced with the increase of inlet velocity and the decrease of melt undercooling. Moreover, the effect of melt flow becomes more significant as the melt undercooling is lower. The upstream growth in Case II is more significant than that in Case I due to the intersection of two flows from left and top boundaries of the domain. However, with the existence of oblique flow near the dendritic tips at the downstream side, the growth there gets less inhibited compared with that in Case I, especially at the lower melt undercooling.
- (3) At the initial stage of solidification, the columnar dendrite at the upstream side is the first to be inhibited because the solute enriched at the dendrite root is blown up. Subsequently, the growth of columnar dendrite is inhibited in sequence along the flow direction. Secondary dendrite arms are developed and first better at the left side than the right side because of a more disturbance caused by melt flow there. It is observed that secondary dendrite arms become better developed and fatter under melt flow. However, due to being under the more serious inhibition, the secondary dendrite arms of the columnar dendrite at the upstream side are difficult to develop. Under weaker melt flow, columnar dendrites near the outlet can easily break through the blockage of melt flow and achieve better developed structures. The competition between bringing in solute enriched melt from upstream side and carrying away solute rejected at interfaces determines the growth behavior of columnar dendrites. In Case IV with higher inlet velocity, columnar dendrites far from the entrance at bottom wall grow faster than those symmetrically in the right wall, however it is reversed for the left columnar dendrites. Additionally, the columnar dendritic growth is dominated by the effect of melt flow on solute distribution around them, although heat transfer is considered.

Acknowledgements

The authors sincerely acknowledge the financial support from National Natural Science Foundation of China No. 50925415 and Specialized Research Fund for the Doctoral Program of Higher Education of China No. 20130042120042.

Reference

- [1] E.J. Pickering, *ISIJ Int.* 53 (2013) 935–949.
- [2] Y. Natsume, D. Takahashi, K. Kawashima, E. Tanigawa, K. Ohsasa, *ISIJ Int.* 53 (2013) 838–847.
- [3] C.Y. Wang, C. Beckermann, *Metall. Mater. Trans. A* 27 (1996) 2754–2764.
- [4] C.Y. Wang, C. Beckermann, *Metall. Mater. Trans. A* 27 (1996) 2765–2783.
- [5] C. Beckermann, C.Y. Wang, *Metall. Mater. Trans. A* 27 (1996) 2784–2795.
- [6] C.Y. Wang, C. Beckermann, *Metall. Mater. Trans. A* 25 (1994) 1081–1093.
- [7] R. Tönhardt, G. Amberg, *J. Cryst. Growth* 194 (1998) 406–425.
- [8] C. Beckermann, H.J. Diepers, I. Steinbach, A. Karma, X. Tong, *J. Comput. Phys.* 154 (1999) 468–496.
- [9] X. Tong, C. Beckermann, A. Karma, Q. Li, *Phys. Rev. E* 63 (2001).
- [10] C.W. Lan, C.J. Shih, *J. Cryst. Growth* 264 (2004) 472–482.
- [11] C.C. Chen, Y.L. Tsai, C.W. Lan, *Int. J. Heat Mass Transfer* 52 (2009) 1158–1166.
- [12] G. Zimmermann, L. Sturz, M. Walterfang, J. Dagner, *Int. J. Cast Metal Res.* 22 (2009) 335–338.
- [13] Z.P. Guo, J. Mi, S. Xiong, P.S. Grant, *Metall. Mater. Trans. B* 44 (2013) 924–937.
- [14] M.F. Zhu, D.M. Stefanescu, *Acta Mater.* 55 (2007) 1741–1755.
- [15] N. Al-Rawahi, G. Tryggvason, *J. Comput. Phys.* 180 (2002) 471–496.
- [16] N. Al-Rawahi, G. Tryggvason, *J. Comput. Phys.* 194 (2004) 677–696.
- [17] J. Banaszek, S. McFadden, D.J. Browne, L. Sturz, G. Zimmermann, *Metall. Mater. Trans. A* 38 (2007) 1476–1484.
- [18] Y.H. Shin, C.P. Hong, *ISIJ Int.* 42 (2002) 359–367.
- [19] M.F. Zhu, S.Y. Lee, C.P. Hong, *Phys. Rev. E* 69 (2004).
- [20] M.F. Zhu, T. Dai, S. Lee, C.P. Hong, *Sci. China, Ser. E: Eng. Mater. Sci.* 48 (2005) 241–257.
- [21] M.F. Zhu, T. Dai, S.Y. Lee, C.P. Hong, *Comput. Math. Appl.* 55 (2008) 1620–1628.
- [22] M.F. Zhu, S.Y. Pan, D.K. Sun, H.L. Zhao, *ISIJ Int.* 50 (2010) 1851–1858.
- [23] D.K. Sun, M.F. Zhu, S.Y. Pan, D. Raabe, *Int. J. Mod. Phys. B* 23 (2009) 1609–1614.
- [24] D.K. Sun, M.F. Zhu, C.R. Yang, S.Y. Pan, T. Dai, *Acta Phys. Sin.* 58 (2009) S285–S291.
- [25] C.R. Yang, D.K. Sun, S.Y. Pan, T. Dai, M.F. Zhu, *Acta Metall. Sin.* 45 (2009) 43–50.
- [26] D.K. Sun, M.F. Zhu, S.Y. Pan, D. Raabe, *Acta Mater.* 57 (2009) 1755–1767.
- [27] D.K. Sun, M.F. Zhu, S.Y. Pan, C.R. Yang, D. Raabe, *Comput. Math. Appl.* 61 (2011) 3585–3592.
- [28] D.K. Sun, M.F. Zhu, T. Dai, W.S. Cao, S.L. Chen, D. Raabe, C.P. Hong, *Int. J. Cast Metal Res.* 24 (2011) 177–183.
- [29] D.R. Liu, E.J. Guo, L.P. Wang, F.W. Kang, Q. Lan, *Int. J. Cast Metal Res.* 20 (2007) 254–264.
- [30] H. Yin, S.D. Felicelli, L. Wang, *Acta Mater.* 59 (2011) 3124–3136.
- [31] B. Jelinek, M. Eshraghi, S. Felicelli, J.F. Peters, *Comput. Phys. Commun.* 185 (2014) 939–947.
- [32] L. Nastac, *Acta Mater.* 47 (1999) 4253–4262.
- [33] L. Beltran-Sanchez, D. Stefanescu, *Metall. Mater. Trans. A* 34 (2003) 367–382.
- [34] L. Beltran-Sanchez, D. Stefanescu, *Metall. Mater. Trans. A* 35 (2004) 2471–2485.
- [35] Y.F. Shi, Q.Y. Xu, B.C. Liu, *Acta Phys. Sin.* 60 (2011).
- [36] X.F. Zhang, J.Z. Zhao, *Acta Metall. Sin.* 48 (2012) 615–620.
- [37] D.M. Li, R. Li, P.W. Zhang, *Appl. Math. Model.* 31 (2007) 971–982.
- [38] L. Yuan, P.D. Lee, G. Djambazov, K. Pericleous, *Int. J. Cast Metal Res.* 22 (2009) 204–207.
- [39] L. Yuan, P.D. Lee, *Modell. Simul. Mater. Sci. Eng.* 18 (2010) 055008.
- [40] S. Karagadde, A. Bhattacharya, G. Tomar, P. Dutta, *J. Comput. Phys.* 231 (2012) 3987–4000.
- [41] W.Q. Tao, *Numerical Heat Transfer*, second ed., Xi'an Jiao Tong University Press, Xi'an, 2001.
- [42] J. Lipton, M.E. Glickman, W. Kurz, *Mater. Sci. Eng.* 65 (1984) 57–63.
- [43] S. Luo, M.Y. Zhu, S. Louhenkilpi, *ISIJ Int.* 52 (2012) 823–830.
- [44] S. Luo, M.Y. Zhu, *Comput. Mater. Sci.* 71 (2013) 10–18.
- [45] Y. Meng, B.G. Thomas, *Metall. Mater. Trans. B* 34 (2003) 685–705.
- [46] M. Alizadeh, A.J. Jahromi, O. Abouali, *ISIJ Int.* 48 (2008) 161–169.
- [47] W.L. Wang, M.Y. Zhu, Z.Z. Cai, S. Luo, C. Ji, *Steel Res. Int.* 83 (2012) 1152–1162.
- [48] W.T. Lou, M.Y. Zhu, *Metall. Mater. Trans. B* 44 (2013) 762–782.
- [49] Z.J. Su, J. Chen, K. Nakajima, J.C. He, *Steel Res. Int.* 80 (2009) 824–833.